


Tribological properties of dry sliding wear behaviour for GFRP composite made by hand layup, VARTM and RTM techniques using taguchi and ANOVA approach

Manuneethi Arasu Palanisamy¹ , Neelamegan Sengodan²

¹Aishwarya College of Engineering and Technology, Department of Mechanical Engineering. Erode, Tamilnadu, India.

²K.S.R. College of Engineering, Department of Automobile Engineering. Namakkal, Tamilnadu, India.

e-mail: manuneethi222@gmail.com, megamgct@gmail.com

ABSTRACT

The surface damage wear mechanism of GFRP is complex in real time applications due to the anisotropic nature of the material. The main objective of this study is to identify the parameters that affect the wear behavior of GFRP composite made by Hand Layup, VARTM and RTM technique. Most GFRP research has focused on fiber/matrix types, but this current research addresses on critical research gap i.e., fiber volume fraction Vf% and optimizing various wear parameters such as load, sliding distance and sliding velocity in order to understand the wear contribution. The result of L9 orthogonal array under dry sliding wear experiment using pin – on – disc tribometer is analyzed by taguchi and ANOVA to determine the optimal wear rate by considering the smaller the best attribute. The result shows that by increasing fiber volume Vf% up to 7% minimum wear rate is observed in materials produced by VARTM and RTM technique. It is evident that improvement of fiber volume in GFRP increases the wear resistance and produce preferential wear with negligible de-bonding of the reinforcement as per SEM study.

Keywords: Dry sliding wear; Hand layup; VARTM; RTM; Taguchi & ANOVA.

1. INTRODUCTION

FRP composite materials are popular in automobile, shipbuilding, air craft and many other industries mainly with advantages such as lightweight, high strength to its weight ratio [1, 2]. In addition, FRP exhibits superior properties such as anti-corrosion resistance, thermal resistance, flexible mechanical properties etc., In most case FRPs are used in surface body structures and their material properties are limited to the range of composition range of reinforcement and matrix [3, 4]. The life of an FRP material and its dimensional stability are determined by the type of raw material, quality of the material and mainly depend on the manufacturing method by improving the fiber quantity [5]. The main objective of this research is to investigate the optimal parameters and improve the quality by reducing wear tribology through increasing fiber content in the in GFRP [6, 7].

Improvement in sliding wear resistance is important because dry friction and wear roots to major issue in repair and product replacement, and this is a key issue in many engineering application [8–11]. However, industries require better tribological property in FRP and this is mainly due to problem faced by material surface wear. The demand for FRP is increasing based on economic and market dynamics, the need for superior wear resistance based on increasing fiber volume fraction and reducing void [12]. Even though relative wear resistance increases irrespective of specific surface area, surface contact but fiber volume fraction directly influences the amount stress level on wear and material fatigue. This is mainly because increasing the percentage of fiber reinforcement improves stiffness and strength [13–15]. From this observation and review of the additional scientific article shows that very limited investigation has been carried out from the reinforcement of fiber volume fraction vf% by varying manufacturing technique [16, 17]. The study of fiber volume fraction vf% irrespective of tribological analysis is an important research gap in recent studies irrespective of improve wear resistance by varying manufacturing technique by minimizing void [18–21].

The review of scientific literature shows that, many articles are not examined the competitiveness of FRP manufacturing method with respect to tribological property [22–25]. A scientific methodology and techniques are necessary to investigate the diverse process factor for wear tribological characteristics of

FRP material. Wear property depends on the mechanical properties like material hardness, stiffness, surface roughness, strength [26]. Improving the wear resistance in FRP material is depends on manufacturing technique by increasing the fiber aspect ratio in the composite [27, 28]. The wear behaviour is improved with respect to the microstructures and this microscopic study can be used to determine the wear surface contact temperature response in relation to the softening of surface contact material under wear [29]. Glass fiber reinforced polymers GFRP is widely used in many applications due to its cheap cost and excellent stability [30]. In most case epoxy resin are used in reinforcement but alternative resin such as isophthalic polyester resin is used in this study due to its cheap cost and high thermal stability.

In this study, the widely used FRP manufacturing Hand layup (HL) techniques is comparatively investigated with vacuum assisted resin transfer molding (VARTM) and resin transfer molding (RTM) technique with respect to quality by determining wear parameter optimization such as design of experiments (DOE) to produce improved quality material [31]. This method determines the DOE, conduct experiments and validate the model to measure the least wear rate through the response. The selection of parameters is based on standard wear laws, i.e. wear rate is directly proportional to normal force, distance and inverse to hardness and soft contact [32, 33]. Taguchi's optimization technique is used in this study, this experimental design eliminates unnecessary repeated tests and determine the acquire parameter influence the significance and variations [34, 35]. Additionally, this wear rate outcome is validated with the help of ANOVA (Analysis of Variance) and regression line value analysis [36]. The broken specimens from pin-on-disc tribometer are observed under SEM to identify the morphological observation which is high effective method to determine the wear and material fracture behaviour.

2. MATERIALS AND METHODS

2.1. Composite preparation

The Synthetic E-Glass fibers made of silica components and thermoset type isophthalic polyester resin are reinforced to form GFRP composite samples. The fiber acts as the primary load-carrying material, where resin act as the bonding material. This combination cerats an anisotropic character for GFRP. 300 GSM (grams per square meter) E-Glass woven fabrics with density of 1.42 g/cm³ and isophthalic polyester resin (NRC 220) with density of 1.1 g/cm³ with additions catalyst MEKP (Methyl ethyl ketone peroxide) and cobalt naphthenate accelerator are used. The ingredient is mixed under standard room temperature 25°C with optimum ratio of 1:0.025:0.015 recommend by the researchers.

In this study, three different manufacturing methods are used for GFRP production namely traditional hand layup (HL), VARTM and RTM method as shown in Figure 1. The HL fabrication process begins with applying the release agent PVA (Poly Vinyl Alcohol) to the mold surface. Impregnated layers of fibers were placed one on top of another on the mold (30 cm × 30 cm) dimension and isophthalic polyester resin was added between woven and pressed as showed in Figure 1a. The hot wet part is allowed to cool for one hour before curing at room temperature for 24 hours and the part is removed. Uniform thickness of 3 mm is maintained using spacers on the mold. The VARTM and RTM techniques begin with placing multiple layers of fibers on one-sided of the mold and closed and tightly sealed with a vacuum bag for VARTM and mating mold for RTM as showed in Figures 1b and 1c. For the VARTM resin infusion process, resin flows through the distribution media and fiber layers with an injection pressure of 25psi through a vacuum pump with fiber- resin ratio of 1:0.45.

The Pressurized resin injected for RTM is carried out with 58–87psi, i.e., 4-6 bar pressure pump is used to inject resin-catalyst mixture into the runner and excess resin is discharged from the riser setup. Vf% is calculated by Equation (1) and Equation (2) where vf and vm are the volume of fiber and matrix and Vf and Vm are volume



Figure 1: (a) HL based GFRP production, (b) VARTM based GFRP production and (c) RTM based GFRP production.

fraction of fiber and matrix and are shown in Table 1. The Barcol hardness test value for HL, VARTM and RTM is measures to be 38, 43 and 42 HRB.

$$V_f + V_m = 1 \quad (1)$$

$$V_f = \frac{v_f}{v_m} \quad (2)$$

2.2. Sliding wear test and Taguchi- ANOVA optimization technique

Wear tests were carried out on a pin on disc testing tribometer according to ASTM G 99-95 standard. The machine consists of fixed pin sliding on EN32 steel rotating disc connected to an electric motor. Specimens of 10 mm × 10 mm × Actual thickness are fixed flat on the sliding pin so that specimen can be in contact the rotating disk showed in Figure 2a. The actual thickness for GFRP is 3 mm for HL and 2.9 mm for VARTM and RTM. The thickness variations occur during the compression operation in VARTM and RTM technique. The change in wear, sliding distance is recorded in LABVIEW software and the total wear rate of the specimens is measured by the difference in the weight of the specimens before and after wearing the test specimens Figures 2b and 2c. The wear rate is determined irrespective of finding the wear co efficient the following Equation (3), Wv represent volumetric wear, K for wear co efficient, P is applied load, S is the sliding velocity.

$$\text{wear co efficient } K = W_v/H/PS \quad (3)$$

The damaged wear broken specimens are examined using microscope and SEM. The investigation of surface wear properties is an important to determine the internal behavior of material under stress. GFRP quality can be easily determined by this surface examination. The high magnification observation such as SEM is necessary to study the surface morphology of the GFRP composite material. The ratio of length to fiber diameter, i.e., the GFRP fiber aspect ratio is considers in many wear studies because GFRP has high aspect ratio, but in terms of FRP production flexibility the fiber volume fraction should be considered.

In this study, the L9 orthogonal array is chosen for the specific factorial design to simplify parameterization. The similar experiments is omitted for repeated testing and the results interpretation is closed with three major parameters namely load, sliding speed and sliding distance considered as shown in Table 2 and Table 3. The Taguchi systematic approach is used to determine the significance of the parameter, which separates the arrays of process parameter by differentiating the levels in orthogonally. This algorithm consisted nine rows and controlled data collection was carried out. The S/N ratio is derived from significance

Table 1: GFRP manufacturing process.

CONFIGURATION CODE	MANUFACTURING PROCESS	FIBER ORIENTATION	FIBER VOLUME FRACTION (VF%)	THICKNESS (MM)	HARDNESS (HRB)
GFRP-HL	Hand layup	[45/0/90/45]6	45	3	38
GFRP-VARTM	VARTM	[45/0/90/45]6	52	2.9	43
GFRP-RTM	RTM	[45/0/90/45]6	50	2.9	42

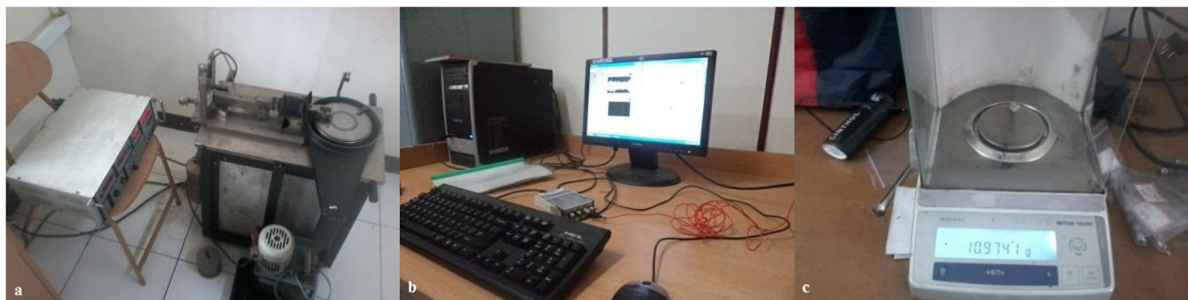


Figure 2: (a) pin on disc testing tribometer, (b) LABVIEW software based wear rate value and (c) Weight measurement to find wear loss.

Table 2: Selected variable levels for wear test.

VARIABLE	LEVEL 1	LEVEL 2	LEVEL 3
load (N)	10	11	12
Sliding velocity (m/s)	2	3	4
Sliding distance (m)	0.6	0.9	1.2

Table 3: L9 orthogonal array for wear test.

LOAD (N)	SLIDING VELOCITY (M/S)	SLIDING DISTANCE (M)
10	2	0.6
10	3	0.9
10	4	1.2
11	2	0.9
11	3	1.2
11	4	0.6
12	2	1.2
12	3	0.6
12	4	0.9

of controllable factors in decibels. Wear response effects are visually identified by mean and S/N ratio graphs, the positive and negative influence is identified by magnitude of effect direction versus slope of the line. The rank compares the relative magnitude of the effect by (Δ) delta if the line is linear. Delta (Δ) is the difference of maximum and minimum S/N ratio. In this wear test, the S/N ratio is selected as smaller the better and calculations are based on Equation (4).

$$\text{S/N ratio (Smaller the better)} = -10 \log_{10} \frac{1}{n} \sum_{i=1}^n y_i^2 \quad (4)$$

ANOVA optimization analysis for wear parameter characteristics is performed by MINITAB software to observe the significant process parameter and contribution. By measuring the mean effect variance, the significant effect of parameter on the quality is investigated and the complexity resulting from the experiments become simple to analyze and are calculate by Equation (5–8).

S/N ratio is expressed as

$$\overline{S/N} = \frac{1}{9} \sum_1^9 \left(\frac{s}{N} \right)_i \quad (5)$$

SS is the sum of squares

$$SS = \sum_{i=1}^9 \left(\left(\frac{s}{N} \right)_i - \overline{(S/N)} \right)^2 \quad (6)$$

SS_i is the sum of the square for i^{th} parameter

$$SS_i = \sum_{i=1}^3 \left(\left(\frac{s}{N} \right)_{ij} - \overline{(S/N)} \right)^2 \quad (7)$$

Contribution

$$\% \text{Contribution} = \frac{SS_i}{SS} \times 100 \quad (8)$$

3. RESULTS AND DISCUSSION

3.1. Signal to noise (SN) analysis on wear behaviour

The variety of tribological factors affect the wear rate that can be easily investigated through DOE array simulation. This leads to reducing the number of experiment runs and guide investigator to achieve the targeted result i.e., minimum wear rate. The L9 is effective balancing orthogonal array is used in this study to identify the impact of three major factors such as load, sliding velocity and sliding distance is taken accounted equally with respect to three levels.

The test result of the wear rate is translated into S/N ratios, which combine results of various parameters. The wear test result is used to determine the S/N ratio to produce the high quality material. Calculation of wear loss calculated is found to be directly proportional to performance of the frictional material. Considering smaller wear rate is best attribute, the experimental results are converted into ratios to measure quality characteristics. The Table 4 shows the wear rate and S/N ratio of various composites and consequently the wear loss increases with increasing load.

The optimal minimum wear rates are observed at load 10N, sliding distance 1.2 m and sliding velocity 4 m/s for VARTM and RTM specimens. HL specimens the minimum wear rate is observed at load 11N, sliding distance 0.6 m and sliding velocity 3 m/s. All the GFRP specimens the maximum wear rate observed at load 12N, sliding distance 1.2 m and sliding velocity 3 m/s. VARTM and RTM based specimen shows significant improvement in wear resistance behaviour compared to wear rate of HL specimens.

The Figures 3, 4 and 5 shows the factors affecting the optimal process parameter to achieve lowest wear rate irre. The mean effect plot for S/N ratio as in right side of Figures 3, 4 and 5 shows that, the slope of the lines indicates the influence of each parameters and the graph indicates. The maximum straightest line and its linearity in lines show the most significant factors. From the right side of Figures 3, 4 and 5 it shows load is the primary factor affecting the wear rate. The Sliding distances shows second linearity for VARTM and RTM specimens.

Left side of Figures 3, 4 and 5 the probability plot analysis for all the samples shows that wear parameters plot wear loss point is closer to the centre mean line and all the points lie in the mean value, that is, the parameter selected for the wear test is valid for all the specimens. The main control parameter is determined by the delta value. This delta is the different between mean high and low characteristics S/N ratio average for the particular factor. In terms of delta, the highest impact parameter is determined for the process parameter, and the ranking is calculated by the highest delta value. The greater delta shows the highest ranking, indicating that factor has a greater influence on the wear rate.

The response to the S/N ratio for hand layup, VARTM and RTM specimens are tabulated in Tables 5, 6 and 7. It shows that, all three groups of specimens are mainly affected by primary load and secondary sliding distance for VARTM and RTM, but HL sliding velocity is second most significant factor as per delta value.

3.2. Interaction plot for wear rate analysis

The interaction of wear related parameters determine the non-parallel factor behaviour through minor correlation as shown in Figures 6, 7 and 8. Compared to other factors, the normal force with respect to applied load on the specimen is high significant factor in determining the wear rate. Sliding velocity is the secondary most

Table 4: Wear rate and S/N ratio result of HL, VARTM and RTM specimens by L9 orthogonal array.

LOAD (N)	SLIDING DISTANCE (M)	SLIDING VELOCITY (M/S)	WEAR RATE HL	WEAR RATE VARTM	WEAR RATE RTM	S/N RATIO HL	S/N RATIO VARTM	S/N RATIO RTM
10	0.6	2	1.97	2.15	2.06	28.44	25.87	26.92
10	0.9	3	1.86	1.86	1.76	51.18	53.32	47.89
10	1.2	4	2.11	1.27	1.35	56.97	49.73	56.12
11	0.6	3	1.81	1.87	1.91	30.77	33.61	30.17
11	0.9	4	1.96	2.20	2.31	28.21	25.91	26.81
11	1.2	2	3.67	3.51	3.25	22.27	18.17	21.71
12	0.6	4	2.06	2.16	2.23	28.93	32.17	29.76
12	0.9	2	4.29	4.16	4.25	15.17	22.18	15.96
12	1.2	3	5.82	4.71	5.07	20.12	18.03	19.97

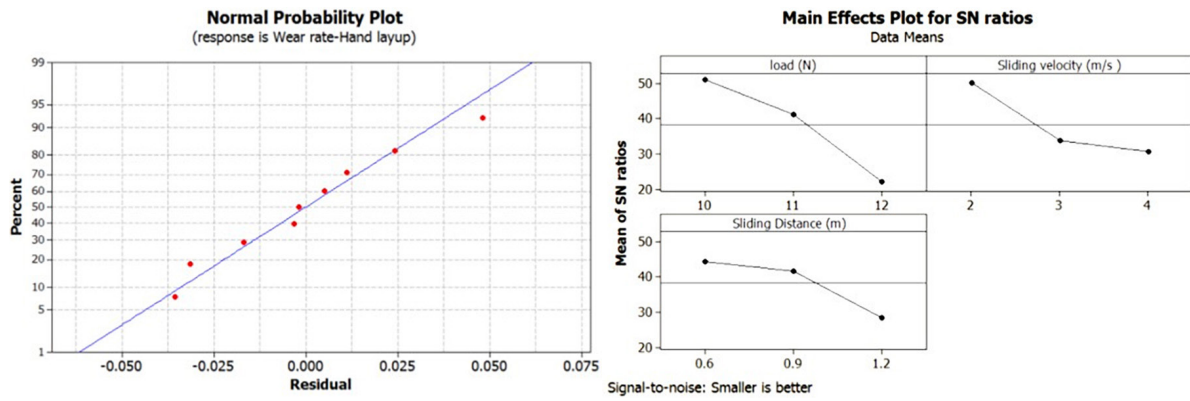


Figure 3: Mean effect plot- S/N ratio for HL specimens at right side and normal probability plot for HL specimens at left side.

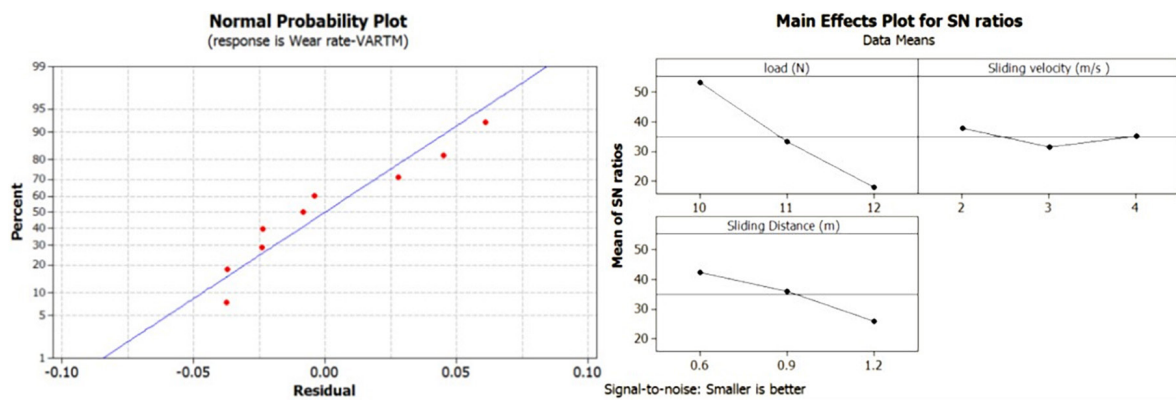


Figure 4: Mean effect plot- S/N ratio for VARTM specimens at right side and normal probability plot for VARTM specimens at left side.

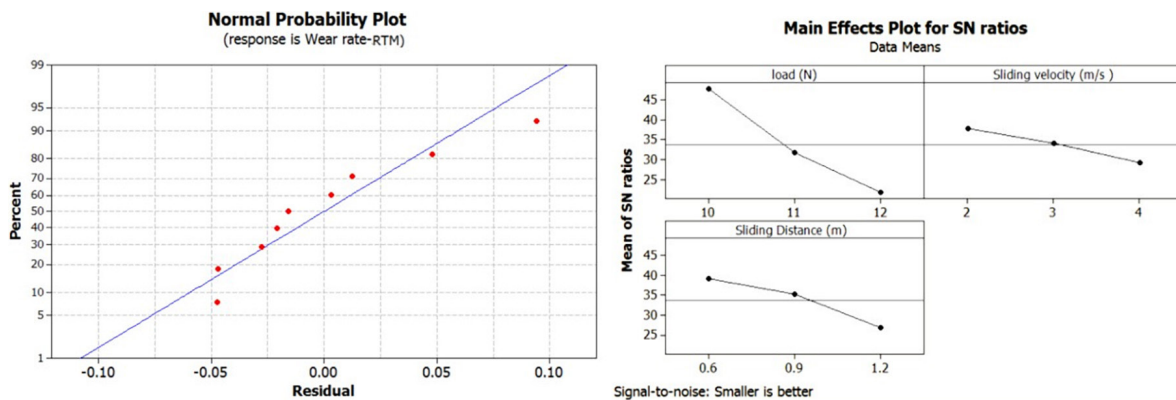


Figure 5: Mean effect plot- S/N ratio for RTM specimens at right side and normal probability plot for RTM specimens at left side.

interaction factor with line linearity for VARTM and RTM specimens as shown Figures 7 and 8. But the sliding distance acts as a second contribution factor in the HL specimen according to an interaction plot with perpendicular lines as per Figure 6.

3.3. ANOVA analysis of wear behaviour

The effect of different variables on wear response is determined by ANOVA method of analysis. The result findings of the L9 array are calculated to determine the percentage of contribution of factor with respect to wear

Table 5: Response table for S/N ratios for GFRP Hand layup.

LEVEL	LOAD (N)	SLIDING VELOCITY (M/S)	SLIDING DISTANCE (M)
1	51.16	50.23	44.40
2	41.29	33.72	41.81
3	22.20	30.70	28.44
Delta	28.95	19.52	15.96
Rank	1	2	3

Table 6: Response table for S/N ratios for GFRP VARTM.

LEVEL	LOAD (N)	SLIDING VELOCITY (M/S)	SLIDING DISTANCE (M)
1	53.29	37.90	42.53
2	33.36	31.36	34.35
3	16.19	33.57	25.95
Delta	37.11	6.54	16.58
Rank	1	3	2

Table 7: Response table for S/N ratios for GFRP RTM.

LEVEL	LOAD (N)	SLIDING VELOCITY (M/S)	SLIDING DISTANCE (M)
1	47.82	37.94	39.13
2	31.79	34.20	35.39
3	21.74	29.21	26.83
Delta	26.08	8.73	12.30
Rank	1	3	2

loss as showed in Tables 8, 9 and 10. The mean difference and estimate process from ANOVA table show the greater influence on the result by determining the statistical significant. The ANOVA analysis mainly consists of F the factor value and P the probability value. The F value is calculated as the difference between the specimen divided by the specimen average, and the higher F value indicates higher parametric significance. The F Value is inversely proportional to the p value, and this P value is calculated by the changes in error. It is indicated from the table that the most significant influence parameter of wear loss is load with delta value of 26.08-37.11. In addition, load shows the most contributed factor among the entire specimen. The rate of wear is majorly affected by the increase in applied load or force.

The load shows 92% and 85% of the major contribution for VARTM and RTM in Tables 9 and 10. Sliding velocity is the second contribution factor to wear rate in HL models, but VARTM and RTM specimen shows a minor significant in sliding distance as the second contribution factor and negligible contribution in sliding velocity. Although the GFRP raw material is similar, the manufacturing technique determines the quality of the material. Table 8 shows, Factors affecting the wear rate of HL specimens are distributed in the sliding velocity, because the stability of the material decreases under increased sliding velocity and the wear rate increases due to its poor fiber-matrix bonding.

3.4. Microscopic analysis of wear surfaces

After the wear test the GFRP specimens are examined under microscopic test and the surface morphology observations shows the precise reasons for de-bonding of glass fragments as in Figures 9, 10 and 11. Microscopic examination of in Figures 9a and 9b shows large crake on the HL material. High contact stress and frictional heat

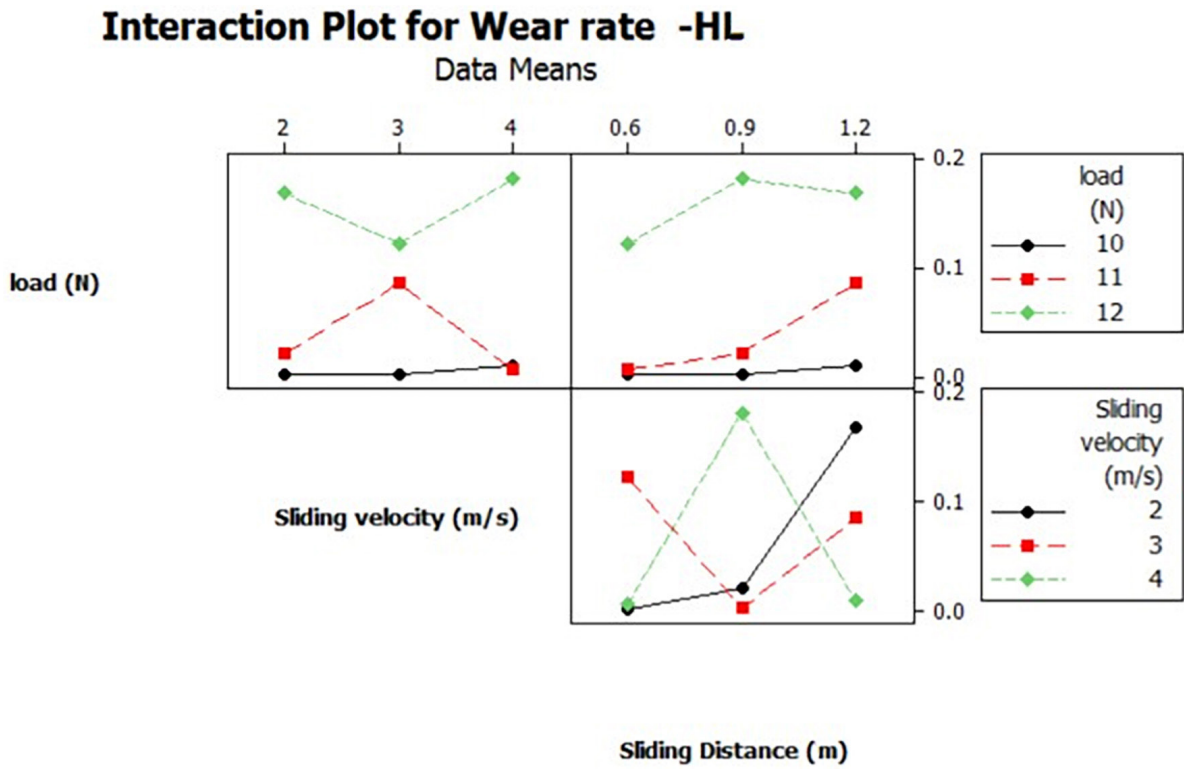


Figure 6: Interaction plot for wear rate for HL specimens.

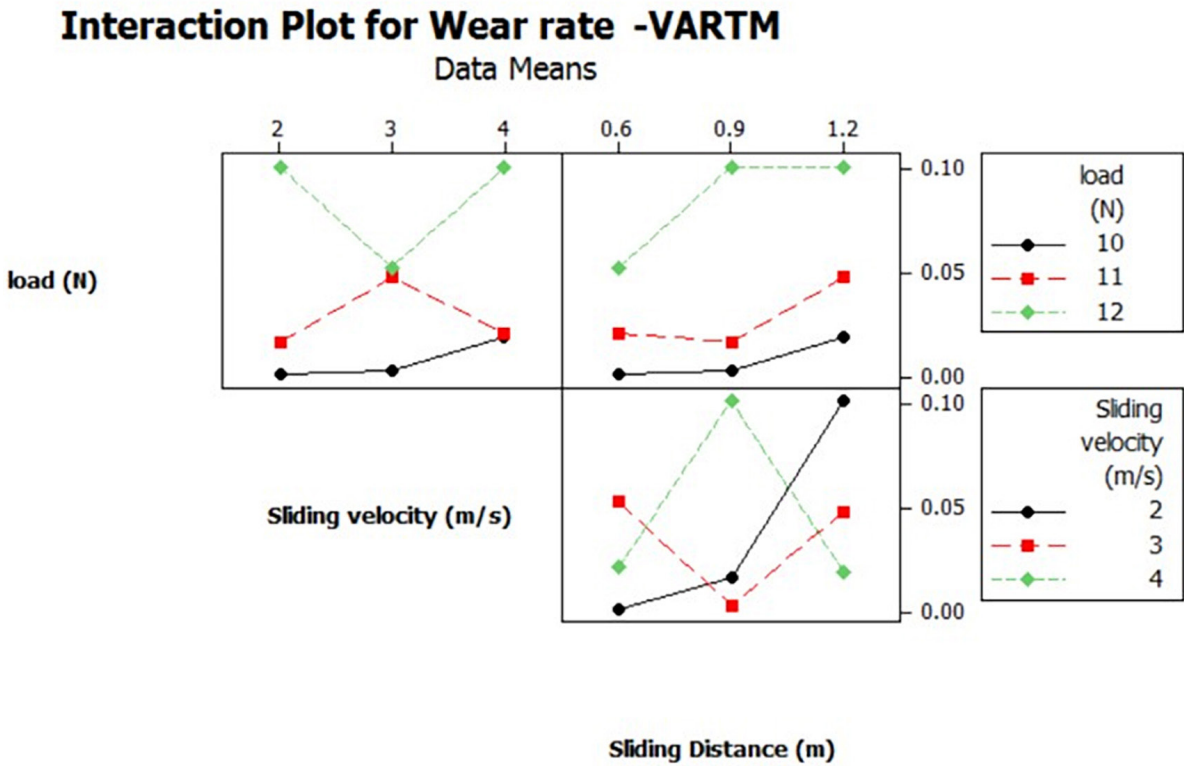


Figure 7: Interaction plot for wear rate for VARTM specimens.

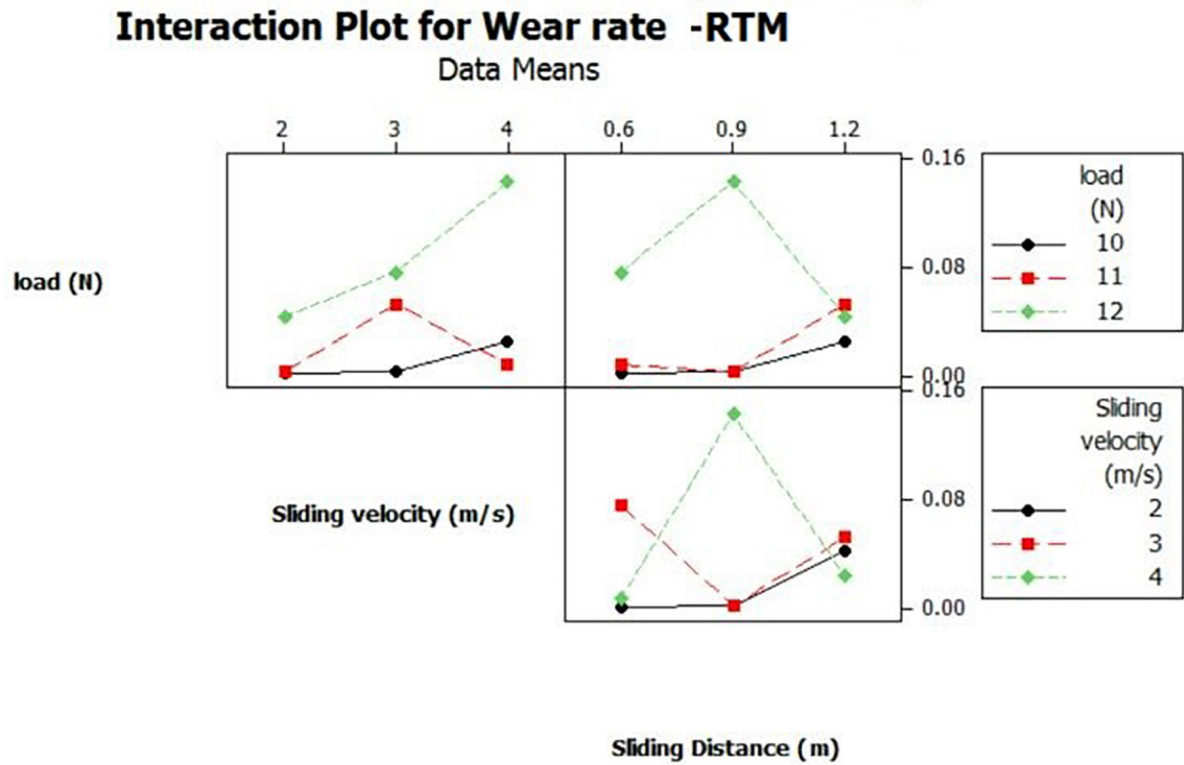


Figure 8: Interaction plot for wear rate for RTM specimens.

Table 8: Contribution of process parameters for GFRP HL.

SOURCE	SUM OF SQUARES (SSI)	%CONTRIBUTION
Load (N)	0.010764	75.199
Sliding velocity (m/s)	0.002878	20.1061
Sliding distance (m)	0.000672	4.6947

Table 9: Contribution of process parameters for GFRP VARTM.

SOURCE	SUM OF SQUARES (SSI)	%CONTRIBUTION
Load (N)	0.039168	92.6596
Sliding velocity (m/s)	0.000065	0.1521
Sliding distance (m)	0.003040	7.19135

Table 10: Contribution of process parameters for GFRP RTM.

SOURCE	SUM OF SQUARES (SSI)	%CONTRIBUTION
Load (N)	0.0096735	85.0417
Sliding velocity (m/s)	0.0002410	2.1186
Sliding distance (m)	0.0014605	12.8395

is the main causes of fiber deboning from the reinforcement in the HL specimen as per Figure 9c. The large size FRP brake from Figure 9a shows that the material has increased with an internal crack at high velocity and the temperature developed at the contact surface affect the adhesion of the material according to SEM Figure 9c and abrasive wear at the end are obtained in HL specimens.

The Figures 10a and 11a from the VARTM and RTM specimens shows high sliding on smooth surface and Figure 10b shows the high abresion reisitance and preferential wear on VARTM model compared to HL specimens Figure 9c. Although smooth slip or sliding occurs on the RTM specimens surface as on Figure 11b, but relatively VARTM Figure 10b shows localized preferential wear with minor de-bonded in GFRP fiber

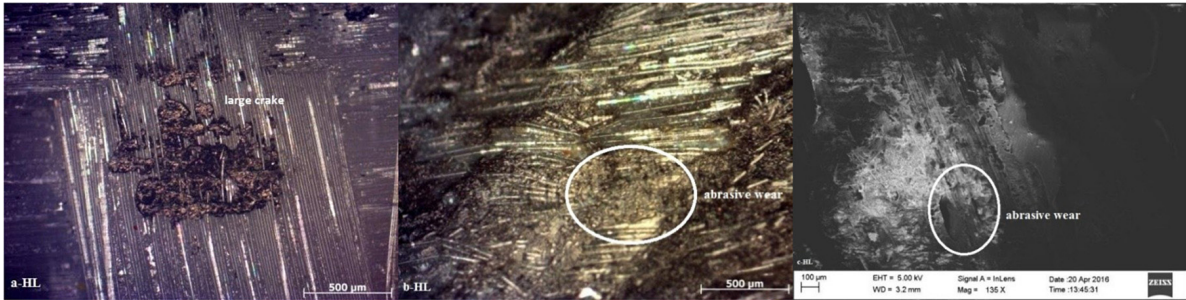


Figure 9: SEM image of HL wear specimen tested under load 12N, sliding distance 0.9m and sliding velocity 2m/s.

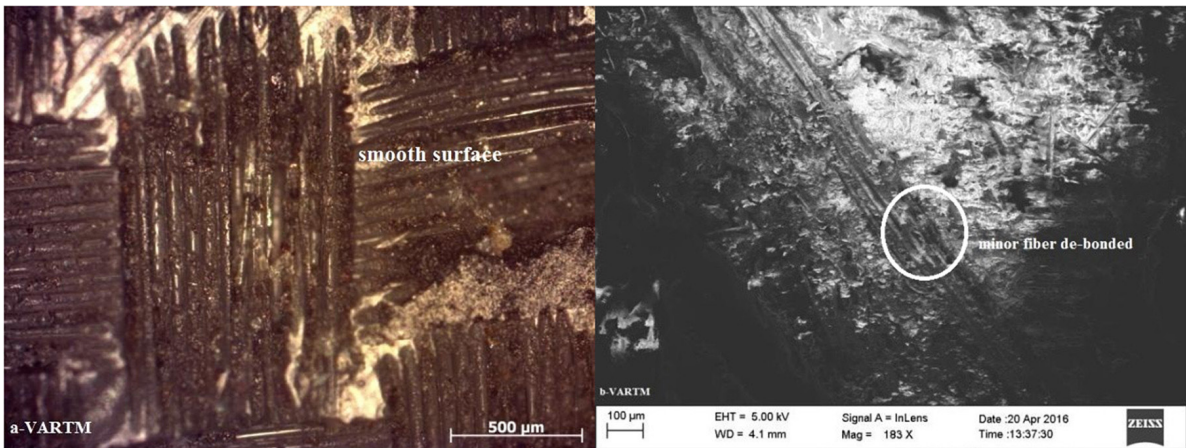


Figure 10: SEM image of VARTM wear specimen tested under load 12N, sliding distance 0.9m and sliding velocity 2m/s.

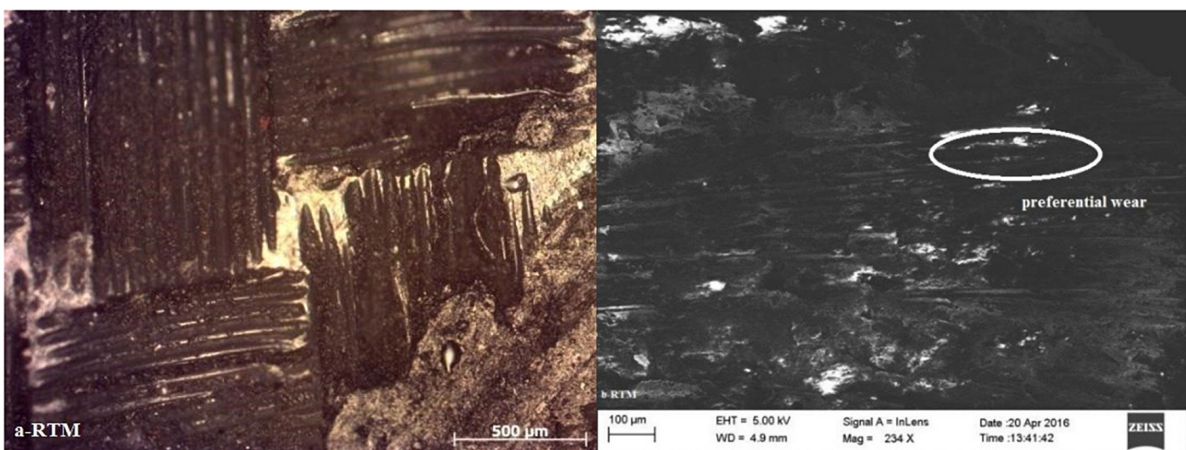


Figure 11: SEM image of RTM wear specimen tested under load 12N, sliding distance 0.9m and sliding velocity 2m/s.

fragments. VARTM samples show high modulus according to higher fiber volume fraction, which is attributed to increase in wear resistance.

Additionally, the increased fiber content in VARTM and RTM showed high adhesion to fiber matrix materials with more surface area contact compare to HL samples. As a result, the wear resistance of GFRP made by VARTM and RTM models is greatly increased. It is evident that an increase in volume fraction decreases the wear rate during sliding.

4. CONCLUSIONS

The following conclusions are drawn from this investigation.

- Although GFRP raw materials are similar, it shows that by changing the production technique which changes the material quality irrespective of change in fiber volume fraction Vf%.
- Considering smaller the wear rate is best attribute in taguchi technique for experimental trail using L9 orthogonal array, it is found that wear loss increases drastically with increase in load.
- According to ANOVA analysis load shows major significant contribution in all specimen groups with 92%–85%.
- VARTM and RTM shows improvement in wear resistance compared to HL specimens as per delta rank. This material has high adhesion to fiber –matrix and form localized preferential wear with minor de-bonding.
- VARTM and RTM interaction plot and ANOVA shows that sliding distance is the second most significant factor, but sliding velocity of HL specimens influence the wear rate secondarily. This in mainly due to poor fiber-matrix bonding in HL specimens, which cause abrasive wear due to frictional heat and internal stress, which causes de-bonding and cracks in the material as per SEM study.
- The minimum optimal wear rate are observed in at load 10N, sliding distance 1.2m and sliding velocity 4m/s for VARTM and RTM samples.

The key findings are that changing the production technique influences the GFRP quality and load is the primary parameter affecting the wear. Strong fiber/matrix bonding, increasing fiber volume fraction, reducing void are the majour influence factors on wear resistance.

5. BIBLIOGRAPHY

- [1] WANG, B., GAO, H., “Fibre reinforced polymer composites”, *Advances in Machining of Composite Materials*, v. 1, n. 1, pp. 15–43, 2021. doi: http://doi.org/10.1007/978-3-030-71438-3_2.
- [2] KUMAR, A., ANANT, R., KUMAR, K., *et al.*, “Anticorrosive and electromagnetic shielding response of a graphene/TiO₂-epoxy nanocomposite with enhanced mechanical properties”, *RSC Advances*, v. 6, n. 114, pp. 113405–113414, 2016. doi: <http://doi.org/10.1039/C6RA15273B>.
- [3] WANG, M., “Developing bioactive composite materials for tissue replacement”, *Biomaterials*, v. 24, n. 13, pp. 2133–2151, 2003. doi: [http://doi.org/10.1016/S0142-9612\(03\)00037-1](http://doi.org/10.1016/S0142-9612(03)00037-1). PubMed PMID: 12699650.
- [4] RAVI, P., ARUMUGAM, E., KATIYAR, J.K., “Investigation of physical, mechanical, tribological and biodegradable properties of hybrid natural fibre reinforced polymer composite”, *Tribology – Materials Surfaces and Interfaces*, 2023.
- [5] HOLMBERG, K., REPONEN, P.K., HARKISAARI, P., *et al.*, “Global energy consumption due to friction and wear in the mining industry”, *Tribology International*, v. 115, pp. 116–139, 2017. doi: <http://doi.org/10.1016/j.triboint.2017.05.010>.
- [6] PAULO DAVIM, J., *Statistical and computational techniques in manufacturing*, Heidelberg, Springer, 2012. doi: <http://doi.org/10.1007/978-3-642-25859-6>.
- [7] PAULO DAVIM, J., *Wear of advanced materials*, London, Wiley, 2011.
- [8] SANJAY, M.R., ARPITHA, G.R., YOGESHA, B., “Study on mechanical properties of natural – glass fibre reinforced polymer hybrid composites: a review”, *Materials Today: Proceedings*, v. 2, n. 5, pp. 2959–2967, 2015. doi: <http://doi.org/10.1016/j.matpr.2015.07.264>.
- [9] KUMAR, S., SINGH, K.K., “Tribological characteristics of glass/carbon fibre-reinforced thermosetting polymer composites: a critical review”, *Journal of the Brazilian Society of Mechanical Sciences and Engineering*, v. 44, n. 11, pp. 496–508, 2022. doi: <http://doi.org/10.1007/s40430-022-03817-z>.

- [10] JAGADEESH, H., BANAKAR, P., SAMPATHKUMARAN, P., *et al.*, “On sliding and abrasive wear behaviour of Bi-directional carbon fiber reinforced epoxy composites”, *Tribology International*, v. 192, pp. 109196, 2024. doi: <http://doi.org/10.1016/j.triboint.2023.109196>.
- [11] PAULO DAVIM, J., *Tribology for Engineers*, Cambridge, Woodhead Pub, 2011.
- [12] ZAGHLOUL, M., STEEL, K., VEIDT, M., *et al.*, “Mechanical and tribological performances of thermoplastic polymers reinforced with glass fibres at variable fibre volume fractions”, *Polymers*, v. 15, n. 3, pp. 694–702, 2023. doi: <http://doi.org/10.3390/polym15030694>. PubMed PMID: 36771995.
- [13] ADERIKHA, V.N., SHAPOVALOV, V.A., “Effect of filler surface properties on structure, mechanical and tribological behavior of PTFE-carbon black composites”, *Wear*, v. 268, n. 11, pp. 1455–1464, 2010. doi: <http://doi.org/10.1016/j.wear.2010.02.022>.
- [14] ZAGHLOUL, M.Y., ZAGHLOUL, M.M.Y., ZAGHLOUL, M.M.Y., “Influence of stress level and fibre volume fraction on fatigue performance of glass fibre-reinforced polyester composites”, *Polymers*, v. 14, n. 13, pp. 2662, 2022. doi: <http://doi.org/10.3390/polym14132662>. PubMed PMID: 35808709.
- [15] ZAGHLOUL, M.M.Y., STEEL, K., VEIDT, M., *et al.*, “Wear behaviour of polymeric materials reinforced with man-made fibres: a comprehensive review about fibre volume fraction influence on wear performance”, *Journal of Reinforced Plastics and Composites*, v. 41, n. 5–6, pp. 215–241, 2022. doi: <http://doi.org/10.1177/07316844211051733>.
- [16] KHODADADI, N., ROGHANI, H., HARATI, E., *et al.*, “Fiber-reinforced polymer (FRP) in concrete: a comprehensive survey review”, *Construction & Building Materials*, v. 432, n. 1, pp. 136634–136652, 2024. doi: <http://doi.org/10.1016/j.conbuildmat.2024.136634>.
- [17] PAULO DAVIM, J., *Design of experiments in production engineering*, Cham, Springer, 2016. doi: <http://doi.org/10.1007/978-3-319-23838-8>.
- [18] MALI, H.S., SHARMA, P., “Machinability of high-strength fiber-reinforced polymer textile composites: a review”, *Mechanics of Composite Materials*, v. 1, n. 1, pp. 1–28, 2023. doi: <http://doi.org/10.1007/s11029-023-10078-x>.
- [19] YANG, B.J., HA, S.K., PYO, S.H., *et al.*, “Mechanical characteristics and strengthening effectiveness of random-chopped FRP composites containing air voids”, *Composites. Part B, Engineering*, v. 62, n. 1, pp. 159–166, 2014. doi: <http://doi.org/10.1016/j.compositesb.2014.02.015>.
- [20] COHEN, D., MANTELL, S.C., ZHAO, L., “The effect of fiber volume fraction on filament wound composite pressure vessel strength”, *Composites. Part B, Engineering*, v. 32, n. 5, pp. 413–429, 2001. doi: [http://doi.org/10.1016/S1359-8368\(01\)00009-9](http://doi.org/10.1016/S1359-8368(01)00009-9).
- [21] GHANI, M.U., AHMAD, N., ABRAHA, K.G., *et al.*, “Review and assessment of material, method, and predictive modeling for Fiber-Reinforced Polymer (FRP) partially confined concrete columns”, *Polymers*, v. 16, n. 10, pp. 1367–1373, 2024. <http://doi.org/10.3390/polym16101367>. PubMed PMID: 38794560.
- [22] LIUJIE, X., DAVIM, J.P., CARDOSO, R., “Prediction on tribological behaviour of composite PEEK-CF30 using artificial neural networks”, *Journal of Materials Processing Technology*, v. 189, n. 1–3, pp. 374–378, 2007. doi: <http://doi.org/10.1016/j.jmatprotec.2007.02.019>.
- [23] JAGADEESH, H., BANAKAR, P., SAMPATHKUMARAN, P., *et al.*, “Influence of nanographene filler on sliding and abrasive wear behaviour of Bi-directional carbon fiber reinforced epoxy composites”, *Tribology International*, v. 192, pp. 109196, 2024. doi: <http://doi.org/10.1016/j.triboint.2023.109196>.
- [24] DIAS, E., CHALSE, H., MUTHA, S., *et al.*, “Review on synthetic/natural fibers polymer composite filled with nanoclay and their mechanical performance”, *Materials Today: Proceedings*, v. 77, pp. 916–925, 2023. doi: <http://doi.org/10.1016/j.matpr.2022.12.059>.
- [25] SHI, J., ZHANG, W., ZHANG, J., *et al.*, “Mechanical, thermal properties and void characteristics of bamboo fiber-reinforced epoxy resin composites prepared by vacuum-assisted resin transfer molding process”, *Journal of Natural Fibers*, v. 20, n. 1, pp. 1–12, 2023. doi: <http://doi.org/10.1080/15440478.2023.2187919>.
- [26] MOHAN, N.S., KULKARNI, S.M., RAMACHANDRA, A., “Delamination analysis in drilling process of glass fiber reinforced plastic (GFRP) composite materials”, *Journal of Materials Processing Technology*, v. 186, n. 1–3, pp. 265–271, 2007. doi: <http://doi.org/10.1016/j.jmatprotec.2006.12.043>.
- [27] BAHRAMNIA, H., SEMNANI, H.M., HABIBOLAHZADEH, A., *et al.*, “Epoxy/polyurethane hybrid nanocomposite coatings reinforced with MWCNTs and SiO₂ nanoparticles: processing, mechanical

- properties and wear behavior”, *Surface and Coatings Technology*, v. 415, pp. 127121–127128, 2021. doi: <http://doi.org/10.1016/j.surfcoat.2021.127121>.
- [28] MOHAN, N., SENTHIL, P., VINODH, S., *et al.*, “A review on composite materials and process parameters optimisation for the fused deposition modelling process”, *Virtual and Physical Prototyping*, v. 12, n. 1, pp. 47–59, 2017. doi: <http://doi.org/10.1080/17452759.2016.1274490>.
- [29] SUBRAMANIYAN, M., KARUPPAN, S., ESWARAN, P., *et al.*, “State of art on fusion deposition modeling machines process parameter optimization on composite materials”, *Materials Today: Proceedings*, v. 45, pp. 820–827, 2021. doi: <http://doi.org/10.1016/j.matpr.2020.02.865>.
- [30] DAS, D., DUTTA, A.K., RAY, K.K., “Correlation of microstructure with wear behaviour of deep cryogenically treated AISI D2 steel”, *Wear*, v. 267, n. 9–10, pp. 1371–1380, 2009. doi: <http://doi.org/10.1016/j.wear.2008.12.051>.
- [31] NAIK, N.K., SIRISHA, M., INANI, A., “Permeability characterization of polymer matrix composites by RTM/VARTM”, *Progress in Aerospace Sciences*, v. 65, pp. 22–40, 2014. doi: <http://doi.org/10.1016/j.paerosci.2013.09.002>.
- [32] PRADHAN, A.K., ALAGIRUSAMY, R., BIJWE, J., “Tribological properties of aramid-polypropylene composites from commingled yarns: influence of aramid fibre weight fraction”, *Journal of the Textile Institute*, v. 100, n. 1, pp. 702–708, 2009. doi: <http://doi.org/10.1080/00405000802170291>.
- [33] ZHANG, X., ZHANG, K., KANG, X., *et al.*, “Friction maps and wear maps of Ag/MoS₂/WS₂ nanocomposite with different sliding speed and normal force”, *Tribology International*, v. 164, pp. 107228–107231, 2021. doi: <http://doi.org/10.1016/j.triboint.2021.107228>.
- [34] SRINIVASAN, A., ARUNACHALAM, R.M., RAMESH, S., *et al.*, “Selection of optimal machining parameters for metal matrix composites using Taguchi Technique”, *Indian Journal of Applied Research*, v. 1, n. 2, pp. 36–38, 2011. doi: <http://doi.org/10.15373/2249555X/NOV2011/12>.
- [35] MURUGESAN, S., NANJUNDAN, K., RAMAN, S., *et al.*, “Investigation and desirability function analysis for optimization of welding process parameters for friction stir welding of aluminium metal matrix composite”, *Warasan Khana Witthayasat Maha Witthayalai Chiang Mai*, v. 49, n. 2, pp. 1405–1415, 2022. doi: <http://doi.org/10.12982/CMJS.2022.089>.
- [36] RAMALINGAM, S., KARUPPUSAMY, A., MAHANDIRAN SUBRAMANIYAM, B., *et al.*, “Green machinability studies on SAE 8822 alloy steel using RSM and taguchi method”, *Matéria (Rio de Janeiro)*, v. 29, n. 2, pp. 1–19, 2024. doi: <http://doi.org/10.1590/1517-7076-rmat-2024-0019>.